

# Aluminum to Aluminum Bonding at Room Temperature

F. Marion, B. Goubault de Brugière, A. Bedoin, M. Volpert, F. Berger, A. Gueugnot, R. Anciant, H. Ribot  
CEA – LETI, MINATEC  
17, rue des Martyrs – 38054 Grenoble Cedex 9, France  
[fmarion@cea.fr](mailto:fmarion@cea.fr), +33 (0) 4 38 78 41 20

## Abstract

In this work we show that high density and very low pitches face to face Aluminum/Aluminum cold bonding is feasible when using Aluminum coated micro-tubes inserted into Aluminum pads.

First, mechanical simulations by FEM show that the insertion pressure felt on the top edge of the Aluminum coated micro-tube is sufficient to break native aluminum oxide present at the interface and also insure the large plastic deformation of aluminum terminations necessary for good electrical and mechanical contact at the joint.

Then an electrical demonstrator with over  $10^6$  connections at a  $10\text{ }\mu\text{m}$  pitch is designed, assembled and characterized: the resistance values of the Al/Al bonds prove to be similar to those obtained with Au/Al bonds.

Ion Beam cross-sections associated with SEM microscopy is used to characterize the morphology of the interface and shows that seamless Al/Al interfaces can be obtained if certain conditions are fulfilled.

Finally the fundamentals of the cold insertion bonding process are discussed and a relationship established with “cold roll bonding” mechanisms, it is shown that the two techniques present some similarities related to very large plastic deformations of bonded materials. This helps us to develop a bonding theory to thoroughly explain the mechanism of the Aluminum/Aluminum bonds formation during the insertion process, as well as its kinematic scenario.

## Introduction

*Applications:* Higher device performance comes with increasing I/O counts, which, when coupled to IC size reduction and 3D integration creates the need for very fine pitch flip-chip technology for inter-stratas connections inside 3D chip stacks. In order to increase density and to reach a  $10\text{ }\mu\text{m}$  or smaller vertical bonding pitch reliable flip chip interconnection technology are needed, in this work we demonstrate that Aluminum to Aluminum (Al0.5Cu) cold bonding technique is a potential candidate.

*Rational for Aluminum / Aluminum cold bonding:* in previous works, connections of Gold coated micro-tubes inserted inside Aluminum (Al0.5Cu) pads have been positively demonstrated (figure 1 & ref. [2, 3]).

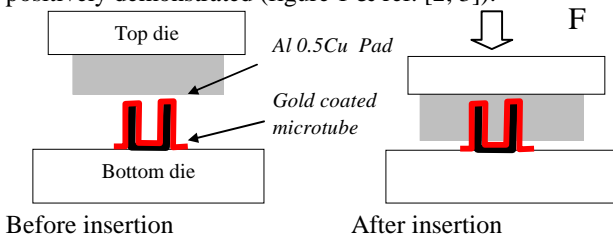


Figure 1: Au/Al bond

In the present study we replace Gold coated micro-tubes by Aluminum coated micro-tubes in order to create a homogeneous and continuous Al0.5Cu interface between the micro-tube and its connecting pad.

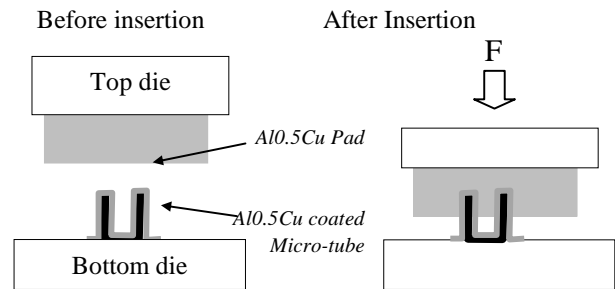


Figure 2: Al/Al bonds

This approach has four major advantages:

a- The material homogeneity of the Al/Al bonds should reduce the inherent reliability concerns present in most other bonding techniques using heterogeneous metal stacks such as “Insertion Bonding” with Au/Al interfaces [1,3], “Copper pillar Solder Bonding” or “Transient Liquid Phase Bonding” (TLP) with various UBM/solder couples. For all these bonding techniques reliability concerns are generally related to intermetallic formation and evolution at the joint frontier.

b- All vertical interconnections inside a 3D stack will have the same thermal budget thanks to the room temperature bonding process.

c- Any Gold processing being eliminated of chip preparation, this process make possible the wafer level fabrication of the micro-tubes and pads through standard BEOL (Back End Of Line) processing lines, where Aluminum is a fully qualified and accepted material.

d- Known Good Dies (KGD) using standard Aluminum pads (without additional chip preparation or post-processes) can be readily flip-chipped over bottom chip or circuit equipped with Aluminum coated micro-tubes.

*Definition of cold Welding:* “Pressure welding utilizes pressure to rupture surface film at the joint interface of two metals and also to extrude virgin metal between islands of surface contamination so that metallic bonding can take place. The process is characterized by high pressure, applied for short periods of time on metal that can be either cold or hot. By necessity bulk plastic deformation of the metals will occur. In pressure welding it is generally accepted that bond formation is controlled by the extent of deformation of the faying surfaces...” [1]. Four consecutive stages characterize any pressure bonding process:

- 1- Removal/breakup of surface oxides or contaminants,
- 2- Contact between regions of uncontaminated metals (virgin metal extrude thru gaps in the ruptured oxide),
- 3- Activation of contacting atoms to form metallic bond (the contact area determines the extent of bonding),
- 4- Atoms re-arrangement as a consequence of heat post-treatments or stress relaxation.

From this general definition we can deduce the definition of “Aluminum/Aluminum cold bonding”:

“It is the process in which two Aluminum (or Aluminum alloys) are pressed one against the other at very high pressure so that it induces such high plastic deformation at the contact junction that native oxide or contaminants readily present on both surfaces are broken and that solid state Al/Al bonds are created at the interface”.

*Applications of cold welding:* two interesting and common industrial applications of pressure welding are “roll bonding” (metal foils assembly) and “wire bonding” (Aluminum to Aluminum wire-bonding is routinely practiced in the semiconductor industry; it utilizes high deformation of an Aluminum bonding wire pressed on an Aluminum pad).

In this later case the Aluminum/Aluminum wire bonded joints are prone to enhanced reliability when compared to Gold/Aluminum wire bonded joints because homogeneous Aluminum bonds are not subject to intermetallic formation related to heterogeneous Gold/Aluminum joints [7].

The use of cold pressure welding has also been proposed for 3D vertical interconnections with various metal combinations:

- Insertion of Gold micro-tubes in Indium or Aluminum pads has been demonstrated [2, 3],
- Low pitch vertical Gold to Gold pressure welding has been demonstrated by Watanabe [5] using cone shaped Gold bumps inserted into doughnut shaped Gold electrode;
- A Copper to Copper cold welding process has been demonstrated by Okoro [6] with the insertion of a Copper bump structure into sloped Copper landing pad (in order to increase significantly local plastic deformation).

### Finite Element Modeling:

*Introduction:* the insertion of Gold coated micro-tubes inside Aluminum (Al 0.5Cu) pads has been modeled in previous works by Finite Element Method (FEM) [4,11], making possible the prediction of the mechanical behavior of the assembly described in figure 1. In the present work we replace the Gold coating on the micro-tube by an Aluminum coating (figure 2). The mechanical modeling of structures involving Aluminum differ of those including Gold because their mechanical characteristics are quite different, especially those related to large plastic deformations, (Table 1)

	E (GPa)	$\sigma_y$ (MPa)	$\sigma_m$ (MPa)	$\nu$
Al0.5Cu	64	110	350	0.35
Au	90	300	825	0.45

**Table 1:** Gold and Al0.5Cu mechanical parameters.

When modeling the insertion described in figure2, we are especially interested in:

- 1 Tracking the plastic deformations of the Aluminum layers on micro-tubes and pads in the first moments of the insertion process.
- 2 Tracking the behavior of the native Aluminum Oxide on the Aluminum pads and micro-tubes.

*Simulation methodology and outputs:* The micro-tube and pad are modeled as a 2D-axisymmetric problem using the “ANSYS” software. Initial geometries are extracted from SEM views of real micro-tubes and pads (Fig 8 and 9). The model construction and boundary condition are described in [11]. Table 1 shows the mechanical parameters used for Aluminum modeling; it is modeled as an elasto-plastic material described using a stress/strain curve based on a logarithmic approximation built on  $\sigma_y$ ,  $\sigma_m$  values issued from table 1 and a non-zero final slope for large plastic deformation (strains up to 1000% are defined).

Figure 3 describes the initial structure before insertion.

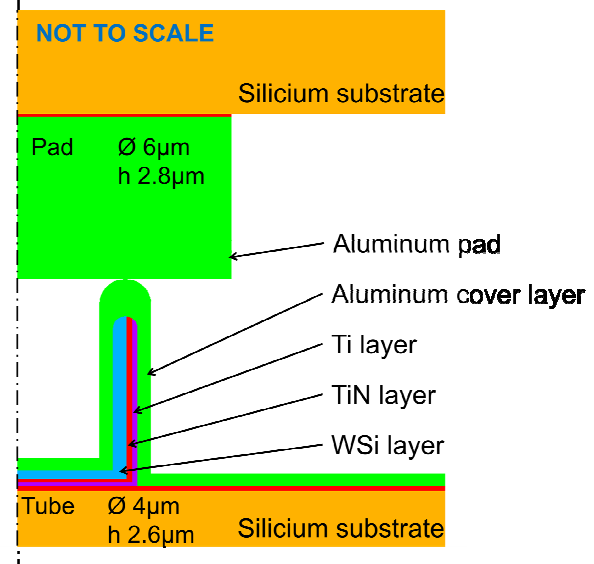


**Figure 3:** Model for the micro-tube insertion,

Now we refer to figure 4 (modeling during insertion) and we define:

- “I” as the “insertion depth= the distance between the flat of the pad and the highest point of the Aluminum cap layer of the micro-tube
- “e” as the “residual thickness of the Aluminum cap layer” (distance between the highest point of the Aluminum cap layer and the highest point of the rigid WSi sub-structure.
- R as the reduction factor (the reduction in thickness of the Aluminum cap layer):  $R = (e_{init} - e_{final}) / e_{init}$ .

*FEM results (1), evolution of the pad shape during insertion:* using the FEM model, the shape of the tube and pad can be tracked and predicted. Figure 4 gives the evolution of pads and micro-tube’s morphologies during the first moments of the insertion process. The top aluminum cap is first deformed up to state **b** where an equivalent plane to plane mechanical contact is reached. Pursuing the insertion through

state **c** conduces to state **d** where an insertion depth of  $I=405\text{nm}$  is reached (note the non-symmetrical deformation of the tube shape due to the proximity of the pad free surface on the right side). In state **d**, Aluminum cap thickness reduction is  $R=70\%$ . Thanks to multiple re-meshing cycles, the plastic deformation has been modeled up to an insertion  $I=0.5\mu\text{m}$ . For deeper insertion depths, the observation of real cases (micro-sections described in the experimental section) takes over and gives the morphological evolution after the present FEM limit is met.

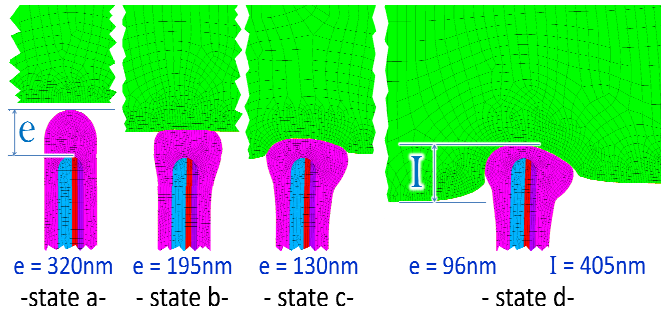


**Figure 4:** Pad and tube deformation at various steps during insertion.

*FEM results (2): prediction of aluminum oxide breakage:* a 3 to 5 nm thick  $\text{Al}_2\text{O}_3$  film is readily present on the micro-tube and pad surface before insertion; it forms naturally after Aluminum deposition when returning to atmosphere. The film is a nonconductive dielectric impeding the formation of an electrical contact between pad and tube at contact. Aluminum oxide is a brittle material with an ultimate tensile strength of 1.5 GPa [12, 13] and an ultimate strain of 1% (a deformation greater than 1% will lead to the film breakage). The ultra-thin oxide layer is not modeled in our Finite Elements Model but we assume that it undergoes the same deformation as the comparatively very thick and ductile Aluminum material present underneath (either on the pad or the micro-tubes). Figure 5 shows the total mechanical strain maps in state **b** and **d**.

In state **b**, the Aluminum strained over 1% is colored orange. If we compare this strain with the ultimate strain of  $\text{Al}_2\text{O}_3$ , we can predict that the dielectric layer broke in the entire contact surface. Pursuing the insertion conduces to very high strains of Aluminum.

In state **d**, the red area endures a strain of over 80 %.: very large islands of Aluminum Oxide free surfaces are present at the interface, they allows to predict that, if an electrical contact is to be formed, that will be in the red contacting areas.

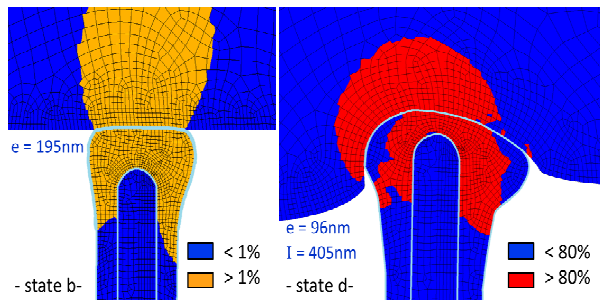


**Figure 5:** Total mechanical strain in the assembly

*FEM conclusion:* the large deformation modeling at the Al/Al interface is a real challenge because it deals with strain ratio largely over 100% and thus requires numerous re-meshing cycles during the solving process.

The model has been used for an insertion up to 450 nm but shows its limit for larger insertion depths, mostly related to re-meshing issues. Until this point, it allows to predict an Aluminum cap layer reduction of  $R=70\%$  for an insertion depth of  $I=405\text{nm}$  (fig. 4) and to predict that an electrical contact may possibly be formed in the red contact areas of figure 5 through largely disrupted  $\text{Al}_2\text{O}_3$  lands

## Experiment

The test vehicle of figure 6 shows the  $\text{Al}_{0.5}\text{Cu}$  coated micro-tubes on bottom chip and  $\text{Al}_{0.5}\text{Cu}$  pads on top chip before insertion, connections yields are electrically tested thanks to daisy chains. Figure 7 is a microscope view of the bottom chip with its peripheral probe pads.

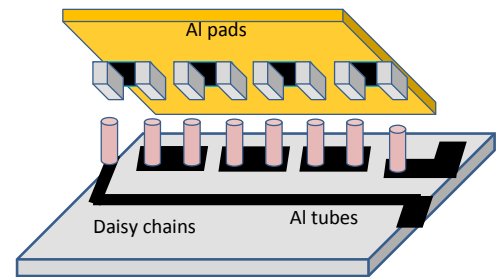


**Figure 6:** Daisy chain measurement

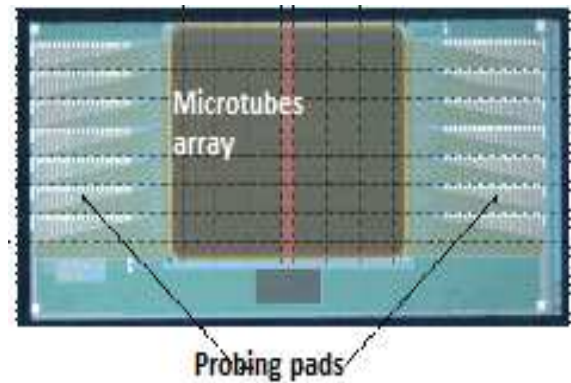


**Figure 7:** Daisy chain measurement

The number of vertical connections is 100 000 at  $10\mu\text{m}$  pitch, the total number of connections addressed by the daisy chains is 9744 (9.7 % of the total connections), they give access to the interconnection yields: % opens, % shorts and vertical resistance of the connection.

*Micro-tube fabrication:* micro-tubes fabrication on 200mm wafers is described in [2]. In the present work  $4\mu\text{m}$  diameter micro tubes are built over a rigid Tungsten Silicide supporting structure, they are  $2.2\mu\text{m}$  high. A 300 nm thick  $\text{Al}_{0.5}\text{Cu}$  cover layer is deposited over the Tungsten “U shaped” micro-tube.

The capping Aluminum layer thickness “e1” at the tip end is measured to be 300nm (FIB  $\mu\text{section}$  + SEM view, fig.8).

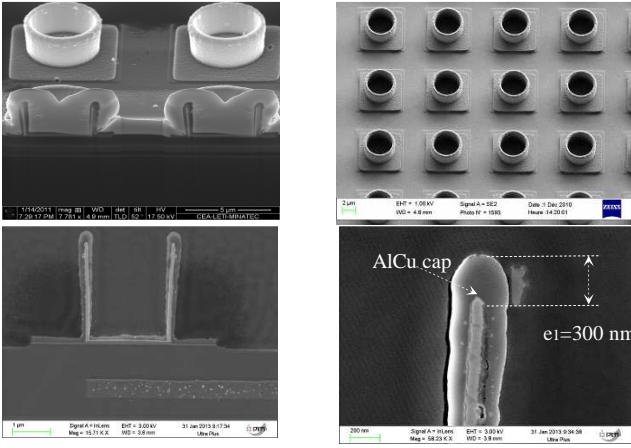


**Figure 8:** Al<sub>0.5</sub>Cu micro-tubes, SEM / FIB  $\mu$ section

**Pads fabrication:** 5.6  $\mu$ m diameters, 2.5  $\mu$ m thick, Al<sub>0.5</sub>Cu cylinders are processed on 200mm transparent wafers using sputter deposition of Al<sub>0.5</sub>Cu layer and standard photolithography tools/techniques for pads definition. Pads are arranged in a 10  $\mu$ m pitch array perfectly matched to the micro-tubes array.

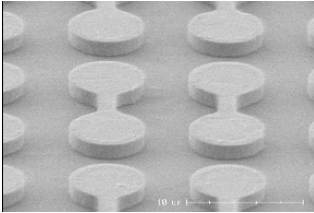


**Figure 9:** Al<sub>0.5</sub>Cu pads, SEM top view

**Bonding:** bonding is performed using an SET's FC300 flip-chip bonder, the experimental design vary the maximum applied load  $F_M$  between two values ( $F_{min}$ ,  $F_{max}$ ) for fixed loading rate  $\dot{F}$  and fixed holding time  $t_h$ . (fig. 10). The interconnection yield, the interconnection resistance and their standard deviation are chosen as responses. Four Al<sub>0.5</sub>Cu capped chips are assembled for electrical testing: 2 chips with 6 mN load per connection, 2 chips with 8 mN load per connection. Top and bottom chips final alignment can be measured thanks to the transparency of the top substrate.

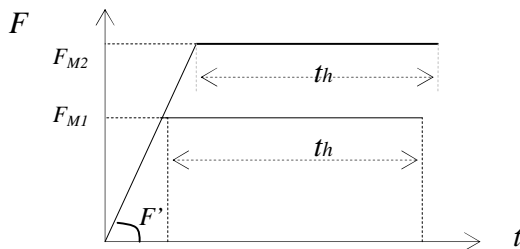


**Figure 10:** Bonding parameters per connection

The mean equivalent stress ( $\sigma_m$ ) is representative of the mean stress at the micro-tube's end at maximum load, it is reported in table1, it is derived from  $\sigma_m = F_m / St$  with  $St$  = projected micro-tube area (area of a micro-tube as physically measured on a SEM top view: fig. 11). It should not be considered in

any case as a "true stress" which is obviously non-uniform as shown in FEM section.

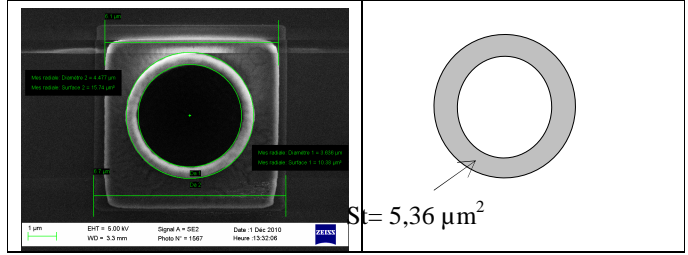


**Figure 11:** projected micro-tube section area

Force $F_m$ (mN)	Number Samples	" $\sigma_m$ " GPa	Ramp $F'$ (mN/sec.)	Holding time (s)
6	2	1,12	0,1	1
8	2	1,49	0,1	1

**Table 2:** Experiment (wafer scale DOE)

The experiments are implemented using a chip to wafer (C2W) assembly technique; the populated wafer is represented in figure 12, each die is inserted with the insertion conditions described in table 2.

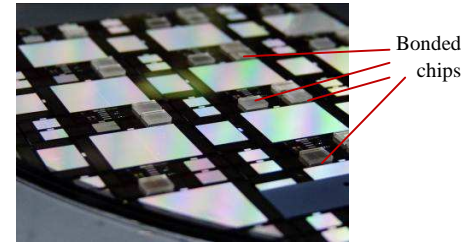


**Figure 12:** Chip to wafer bonding (C2W)

## Experimental Results

**Electrical results:** Connecting yields (opens and shorts) and serial resistances per connection are extracted from probe measurements. 5124 connections per chip are tested to statistically calculate the connection yield, 4620 connections per chip are tested to calculate "shorts" between adjacent connections. The serial unit resistance of each connection is given by the slope of the line plotting chains resistance's versus number of connections per chain (chains of 2, 10, 50 connections). The calculated resistance includes "link resistance" between connections and "access resistance" from link to connection. More precise measurements using arrayed Kelvins are in process in order to extract "pure" vertical connection resistance purged from link and access resistance.

Force (mN)	Ref CH	Yield		Serial resistance per connection	
		Connection Yield mean %	Shorts Defects %	Mean resistance (m $\Omega$ )	Min/Max resistance (green cell only)
8	103	100	0	183	101 / 264
8	104	99.95	0	259	180/620
6	91	88	0	570	160/10330
6	109	55	0	360	180/1670

**Table 3:** Electrical results



Devices CH103, CH104 are inserted with a force of 8 mN per connection; devices CH91 and CH109 are inserted with a force of 6 mN per connection

The “mean resistance” reported in table 3 is the average resistance of all 100% yielding cells (green cells of figure 7 & 8 for example), the “min. Resistance” is that of the lower serial resistance cell, the “max. Resistance” is that of the higher serial resistance cell.

**Discussion on electrical results:** The mean value of the interconnection resistance per connection is 220 mΩ for the 8 mN insertion group, it compares favorably with the resistance of 293 mΩ obtained in previous works for the insertion of 4μm diameter gold coated micro-tube into Al0.5Cu lands [4]. The mean interconnection yield of the high force insertion group is 99,97 %. Inside the “8 mN” group, the device CH103 is totally free of any connection defect (short or open: fig 13), the device CH104 has only one connection opened (one missing chain).

In revenge, the 6 mN insertion group presents very poor interconnection yields (55%, 88%)

Let’s detail now one sample out of each group in order to analyze the dissymmetrical low force/high force electrical results (fig 13: sample processed using high force, fig. 14: sample processed using a too low force). The interconnection map of figure 14 shows clearly identified non-connected areas for a “low force” condition device (red cells represent at least one open chains inside the cell), connection defects are later analyzed then discussed in the “microstructural analysis” section for device CH109.

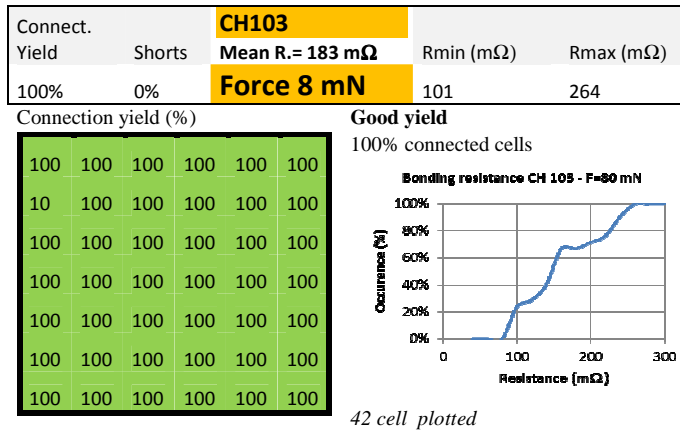


Figure 13: Connection yield/access resistance (8mN)

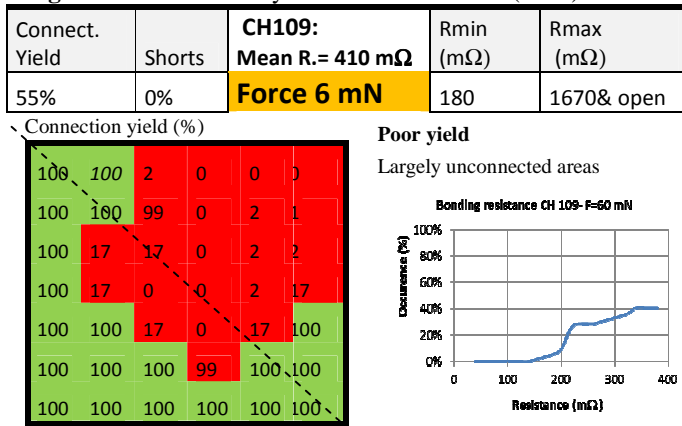


Figure 14: Connection yield/access resistance (6mN)

**Microstructural analysis:** we perform a transversal cross-section analysis of CH109 in order to quantify the frontier between a good and a bad connection. We first establish a link between electrical measurements exposed in figure 14 and microstructural results extracted from the cross-section of sample CH109. Observations are done on this sample in order to determine the physical limit between good and bad connections on a component presenting an evident “too low insertion force” of 6 mN per connection. We use a Triple Ion Beam Cutter (EM TIC3X) from Leica to cut through sample CH109 until we reach the connecting area; then we measure from SEM views of the cross sectioned area the insertion depth “I” and the residual Aluminum cap thickness “e3” at points A,B & C points, as described inside figure 15

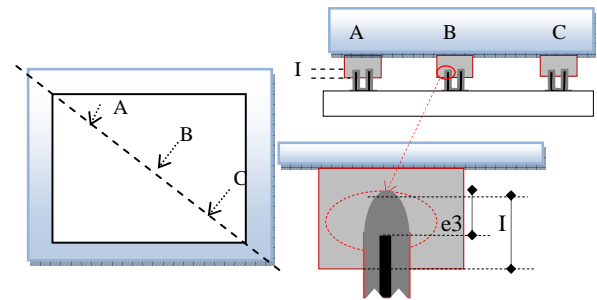


Figure 15: Microstructural analyse : CH109

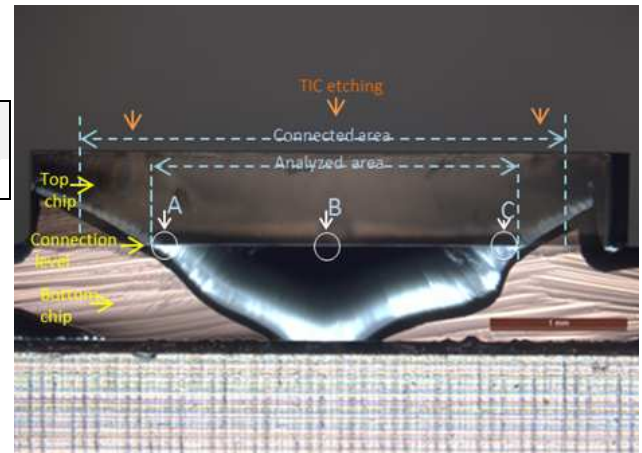


Figure 16: Microstructural analysis: CH109

Table 4 compiles vertical resistance values, insertion depth and reduction factor at point A, B, C.

With, as defined in figure 15:

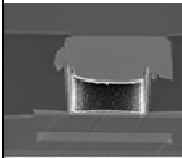
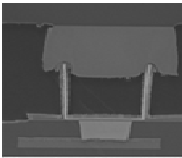
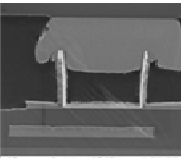
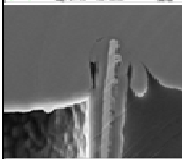
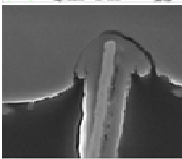
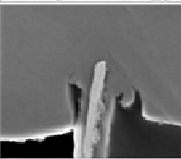
I= Insertion depth extracted from SEM views

R=Reduction factor = (e1- e4) /e1.

- e1=Aluminum cap thickness before insertion (figure 8)

- e4=Aluminum cap thickness after insertion (figure 15)

- Rs= serial resistance measured before cross sectioning of the sample.

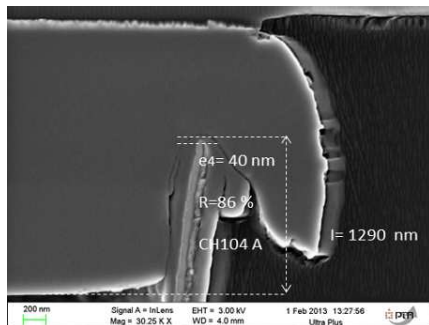
A	B	C
		
		
I= 842 nm e4= 44 nm R= 85%	I= 609 nm e4= 63 nm R= 79%	I= 1058 nm e4= 30 nm R= 90%
Rs= [251-354] mΩ	Poor connection yield /opens	Rs= [178-289] mΩ

**Table 4:** CH109: access resistance (Rs), insertion depth (I) and reduction factor (R)

*Discussion:* first, the compared SEM view of table 4 clearly shows that the electrical contacts are established at the tip of the micro-tube (partial seamless joint frontier).

At point B a low insertion depth is measured (609 nm) and a clear frontier (seam) observed between the Aluminum of the micro-tube and Aluminum of the pad (poor or no measured electrical contact). At point A and C a high insertion depth is measured (842nm, 1058 nm) and a seamless frontier is observed between the Aluminum of the micro-tube and the Aluminum of the pads (good electrical contact measured).

Other cross sections analysis are practiced on CH103 & CH104 which belongs to the 8 mN insertion group (fig. 17, 18), they clearly show that the insertion depth for this group is always above 1000nm for all observation points and that the residual Al0.5Cu layer always remain under 60 nm (i.e.: e4<50 nm, R>83%). They confirm that the electrical contact is established on the top end of the micro-tube (a seamless frontier between Aluminum of the micro-tube and Aluminum of the pad can be observed) and that a solid state Aluminum bond is prone to be established in this area, TEM analysis should confirm these assumptions. In all cases, the initial 300nm high Aluminum cap of the tube (fig. 8) is largely deformed into a “mushroom like” shape, spread out on the internal and/or external sides of the Tungsten Silicide micro-tube’s structuring heart (table 3 & figure 17,18).



I= 1290 nm  
e4= 30 nm  
R= 86%  
Rs= 215 mΩ

**Figure 17:** Microstructural analysis, CH104

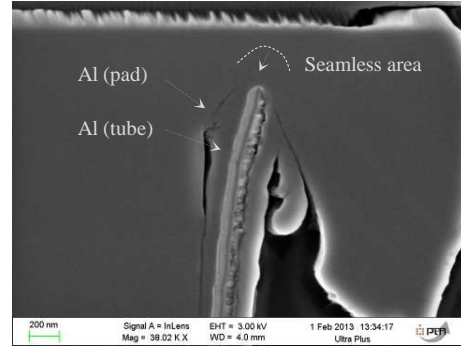


**Figure 18:** Seamless Al / Al frontier, CH104

Based on this full microstructural analysis (4 samples cross-sectioned, three observation points each) and the cross-coupled electrical measurements corresponding to each observation point, we can state that a minimum insertion depth of 800 nm coupled to a minimum deformation ratio R= 83 % are required to insure acceptable connection yields: these morphological conditions are insured by an 8 mN minimum insertion force per micro-tube.

### Discussion:

The FEM simulation section has shown that:

- Native Aluminum Oxide layers starts disrupting when the insertion depth exceeds I=195 nm (orange area of fig.5)
- Large Alumina areas of pure Aluminum lands are opened for I > 405 nm (red area of fig. 5), SEM profiles of the junction around I=500nm confirm that simulated sections are conform to real measured micro-sections (mushroom like shape of the micro-tube’s tips)

Unfortunately, the too large plastic deformations involved over I= 450nm do not yet permit the FEM modeling of deeper insertion depths but the experimental section shows that it can thoroughly complete the morphological study for I>450 nm allowing us to build a first kinetic theory of the bonding process, which is exposed in the next section.

*Bonding mechanism theory:* analogies exist between the “insertion” and the aforementioned “cold roll bonding” mechanisms. Let’s remember that, in the roll bonding process two metal foils are stacked together and then pressed through a pair of rolls until an appropriate deformation is achieved to produce a solid state bonding between the original metal foils [8, 9, 10]. Figure 19 describes this process and summarizes the basic rules that insure good bonding relatively to the reduction factor R (R=reduction in the thickness of the foils), let’s assume the thickness entering rolls is  $e_{in}$ , thickness at the exit is  $e_{out}$ , then  $R = (e_{in} - e_{out}) / e_{in}$ .

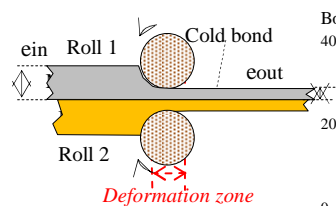


**Figure 19:** roll bonding, & reduction factor

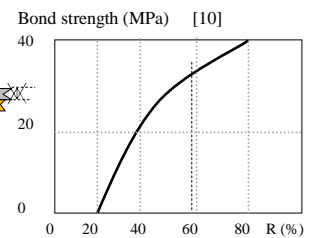


**Figure 20:** bond strength versus reduction factor R for Al foils

Depending on surface preparation, Aluminum to Aluminum roll bonding becomes effective from a minimum reduction factor of 21% (figure 20).

Four different theories have been proposed yet to explain the cold roll bonding mechanisms [8, 10]: the “film theory”, the “energy barrier theory”, the “diffusion barrier theory” and the “recrystallization theory” (or combinations of these).

The “film theory” is the most accepted one; it proposes that the bonding take place in a three stages process through the fracture and extrusion of the work hardened surface layer pressed in contact:

- 1- Physical contact,
- 2- Activation,
- 3- Interaction between bonded materials.

We may extend the roll bonding theory to the Al/Al insertion case, what we propose here is a derived “four steps scenario” for the Aluminum to Aluminum insertion bonding case; this bonding scenario is described in figure 22.

**Step1:** First contact between micro-tubes and top surface of pads.

Insertion depth is zero, the Aluminum thickness covering the micro-tube is  $e_1$  (original film thickness), mechanical contact is established between Aluminum surfaces covered with 5 nm native oxide on each side, no electrical contact is possible

**Step2:** the insertion depth is  $I_2$ .

Aluminum thickness on tube is modified by plastic deformation and reduced to  $e_2$ . Native  $Al_2O_3$  film starts disrupting on the micro-tube and on the pad due to high plastic deformation (as shown by FEM simulation). Very poor / noisy electrical contact can be established (table 3 confirms a poor electrical contact is obtained at point B for our experimental conditions).

**Step3:** the insertion depth is  $I_3$ ;

Aluminum thickness on tube is further modified by plastic deformation and reduced to  $e_3$ . Native  $Al_2O_3$  films disrupt largely on  $\mu$ tube and pads and pure Aluminum extrudes through these disrupted  $Al_2O_3$  lands. Pure extruded Aluminum from pads and micro-tube joins and starts bonding. Larger contact areas and then good serial resistance can be obtained for increased insertion depth  $I$  and reduction factor  $R$  (SEM view point A & C, table 3 confirms). Aluminum both ends fully interacts to build solid state bonds and a good electrical contact is established

**Step4:** thermal annealing may be necessary to complete solid state bonding by diffusion.

This scenario is supported by a good correlation between electrical results (bonding resistance) and microstructural results after insertion (i. e.: insertion thickness and reduction factor) obtained at point A, B, C of the sample CH109 (Table 4).

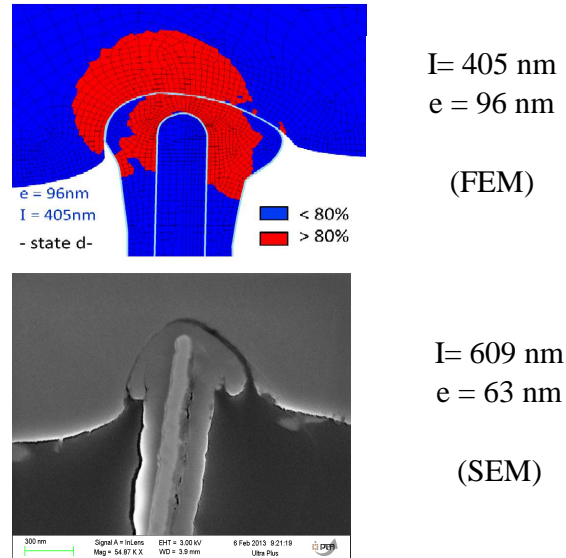


**Figure 21:** comparison of FEM with real cross section

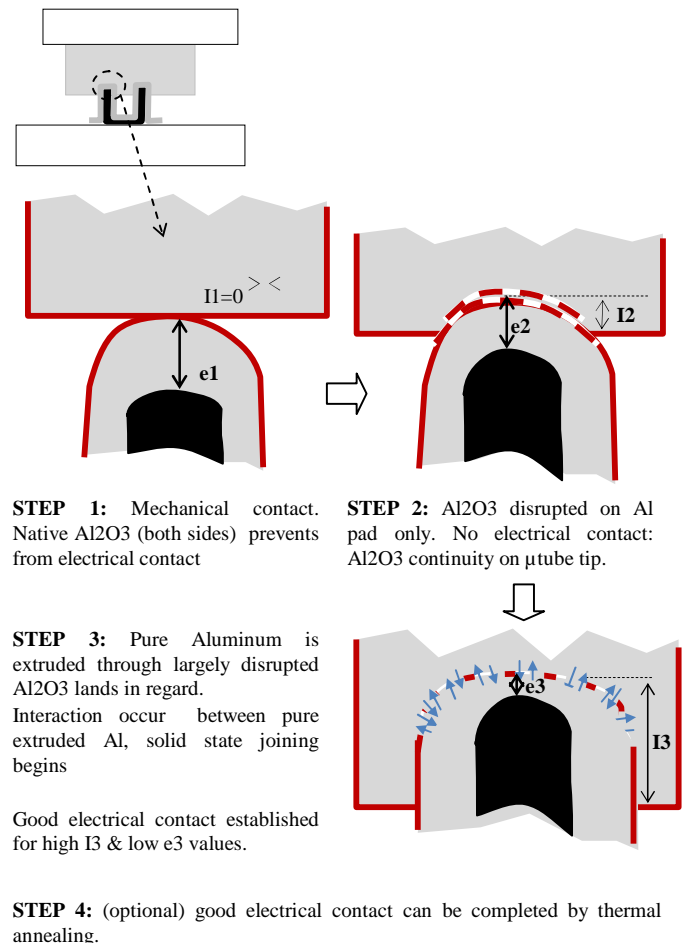


**Figure 22:** an Al/Al bonding scenario

## Conclusions

We have shown that cold Aluminum to Aluminum pressure bonding is feasible under the conditions exposed in this work and for an interconnection pitch of 10  $\mu\text{m}$ .

For the two Aluminum parts to be bonded under compressive pressure, it is imperative that the Aluminum covering layers on the bonded surfaces are fractured to allow fresh material underneath to flow through and create metallic solid state Al/Al bonds

For this to happen it is necessary to create such a plastic deformation of the two parts that the Aluminum cap layer at micro-tube's end is reduced by more than 83% in thickness together with a minimum insertion depth of 1  $\mu\text{m}$ .

Future works will explore:

- Micro-tubes insertion into buried Aluminum pads in order to suppress "pads tearing" that can be observed on cross sections, then force contact areas and finally increase solid state "seamless" bonding areas.
- The development of a pre-applied underfilling process to prepare components to a full reliability thermal/humidity stress cycle.

## Acknowledgments

This work was funded thanks to the French national program 'programme d'Investissements d'Avenir, IRT Nanoelec' ANR-10-AIRT-05.+

## References

1. G. Humpston, D. Jacobson, *Principles of Soldering*, ASM International, Ohio, 2004, pp. 8–9.
2. F. Marion, D. Saint Patrice, M. Fendler et al. "Electrical characterization of high count, 10  $\mu\text{m}$  pitch, room-temperature vertical interconnections". *Proceedings Int. Conf. Device packaging*, Scottsdale AZ, March 2009.
3. B. Goubault de Brugière, F. Marion et al. "A 10 $\mu\text{m}$  pitch interconnection technology using micro tube insertion into Al-Cu for 3D applications". *Proc 61th Electronic Components and Technology Conf*, Lake Buena Vista, FL (2011)-p1400-1406.
4. B. Goubault de Brugière, « Interconnexions haute densité et intégration 3D : étude du contact mécanique et électrique réalisée par insertion de micro-tubes », PhD Thesis, 2012, Université de Lorraine.
5. N. Watanabe, T. Asano, "Room-Temperature Chip-Stack Interconnection Using Compliant Bumps and Wedge-Incorporated Electrodes". *Proc 60th Electronic Components and Technology Conf*, Las Vegas, NV, 2010 p1763-1768.
6. C. Okoro, R. Agarwal, P. Limaye et al. "Insertion Bonding: A Novel Cu-Cu Bonding Approach for 3D Integration". *Proc 60th Electronic Components and Technology Conf*, Las Vegas, NV, 2010-p1370-1375.
7. H. Xu & al. "Intermetallic phase transformations in Au/Al wire bonds", *Intermetallics Vol. 19 (2011) pp1808-1816*.
8. Zhang W., Bay N., "Cold welding,-Experimental investigation of the surface preparation methods" *Welding journal* 1997, vol. 76, no8, pp.326-330.
9. Long Li & al., "Progress in cold roll bonding of metals" in *Sci. technol. Adv Material. Vol9 (2008)*.
10. Eizadjou M., Danesh Manesh H., "Investigation of roll bonding between aluminum alloy strips". *Materials & Design, Volume 29, Issue 4, 2008, Pages 909–913*.
11. B. Goubault, F. Marion & al., Electro-mechanical studies of micro-tube insertion into Al-Cu pads for 10 $\mu\text{m}$  pitch interconnection technology and 3D applications", *Microelectronic Engineering (2013)*.
12. D. Mercier et al., "Investigation of the fracture of thin amorphous alumina films during spherical nanoindentation", *Proceedings of the Nanomechanical Testing Conference, 2012, Lanzarote, Spain*.
13. D. Mercier et al., "Analysis of electrical contact resistance establishment between a Ni microinsert and an Al thin film in flip chip applications", *Materials and advanced metallization", Proceedings MAM conference, 2012, Grenoble, France*.